Magn Reson Med Sci 2018; 17; 138–144
doi:10.2463/mrms.mp.2017-0031
Published Online: December 7, 2017

MAJOR PAPER

The Relationship between Neurite Density Measured with Confocal Microscopy in a Cleared Mouse Brain and Metrics Obtained from Diffusion Tensor and Diffusion Kurtosis Imaging

Ryusuke Irie[1,2*], Koji Kamagata[1], Aurelien Kerever[3], Ryo Ueda[4], Suguru Yokosawa[5], Yosuke Otake[5], Hisaaki Ochi[5], Hidekazu Yoshizawa[6], Ayato Hayashi[7], Kazuhiko Tagawa[8], Hitoshi Okazawa[8], Kohske Takahashi[9,10], Kanako Sato[1], Masaaki Hori[1], Eri Arikawa-Hirasawa[3], and Shigeki Aoki[1]

Purpose: Diffusional kurtosis imaging (DKI) enables sensitive measurement of tissue microstructure by quantifying the non-Gaussian diffusion of water. Although DKI is widely applied in many situations, histological correlation with DKI analysis is lacking. The purpose of this study was to determine the relationship between DKI metrics and neurite density measured using confocal microscopy of a cleared mouse brain.

Methods: One thy-1 yellow fluorescent protein 16 mouse was deeply anesthetized and perfusion fixation was performed. The brain was carefully dissected out and whole-brain MRI was performed using a 7T animal MRI system. DKI and diffusion tensor imaging (DTI) data were obtained. After the MRI scan, brain sections were prepared and then cleared using aminoalcohols (CUBIC). Confocal microscopy was performed using a two-photon confocal microscope with a laser. Forty-eight ROIs were set on the caudate putamen, seven ROIs on the anterior commissure, and seven ROIs on the ventral hippocampal commissure on the confocal microscopic image and a corresponding MR image. In each ROI, histological neurite density and the metrics of DKI and DTI were calculated. The correlations between diffusion metrics and neurite density were analyzed using Pearson correlation coefficient analysis.

Results: Mean kurtosis (MK) ($P = 5.2 \times 10^{-9}$, $r = 0.73$) and radial kurtosis ($P = 2.3 \times 10^{-9}$, $r = 0.74$) strongly correlated with neurite density in the caudate putamen. The correlation between fractional anisotropy (FA) and neurite density was moderate ($P = 0.0030$, $r = 0.42$). In the anterior commissure and the ventral hippocampal commissure, neurite density and FA are very strongly correlated ($P = 1.3 \times 10^{-5}$, $r = 0.90$). MK in these areas were very high value and showed no significant correlation ($P = 0.48$).

Conclusion: DKI accurately reflected neurite density in the area with crossing fibers, potentially allowing evaluation of complex microstructures.

Keywords: *diffusion magnetic resonance imaging, non-Gaussian, histocytological preparation techniques, confocal microscopy, mice, mutant strains*

Introduction

Diffusional kurtosis imaging (DKI) enables sensitive measurement of tissue microstructure by quantifying the non-Gaussian diffusion of water molecules.[1,2] DKI is widely applied in many situations such as brain tumors,[3,4] cerebrovascular disease,[5–10] demyelinating disease,[11,12] hydrocephalus,[13–15] and Parkinson disease.[16,17] Although some studies have reported a relationship

[1]Department of Radiology, Juntendo University School of Medicine, 2-1-1 Hongo, Bunkyo-ku, Tokyo 113-8421, Japan
[2]Department of Radiology, The University of Tokyo Graduate School of Medicine, Tokyo, Japan

*Corresponding author, Phone: +81-3-3813-3111, Fax: +81-3-3816-0958, E-mail: ririe@juntendo.ac.jp

Received: March 6, 2017 | Accepted: September 14, 2017

[3]Research Institute for Diseases of Old Age, Juntendo University Graduate School of Medicine, Tokyo, Japan
[4]Department of Radiological Sciences, Tokyo Metropolitan University Graduate School of Human Health Sciences, Tokyo, Japan
[5]Research & Development Group, Hitachi Ltd., Tokyo, Japan
[6]Department of Plastic and Reconstructive Surgery, Juntendo University Graduate School of Medicine, Tokyo, Japan
[7]Department of Plastic and Reconstructive Surgery, Juntendo University Urayasu Hospital, Chiba, Japan
[8]Department of Neuropathology, Tokyo Medical and Dental University, Tokyo, Japan
[9]Department of Psychology, Chukyo University, Aichi, Japan
[10]Araya Brain Imaging, Tokyo, Japan

between DKI parameters and histological findings,[18,19] a histological foundation for the analysis results of DKI is lacking. As diffusion MRI provides 3D voxel-based data, the information from two-dimensional tissue slices is not sufficient to be used for accurate verification.

Brain clearing is a novel technique to visualize 3D structures inside the brain in great detail.[20] It allows use of a thick (1–2 mm) slice of the sample in confocal microscopy, while a very thin slice of the sample is necessary for analysis with conventional microscopy. The damage by slicing the sample is minimized with a cleared mouse brain.

The purpose of this study was to evaluate for a relationship between diffusion tensor imaging (DTI) and DKI parameters and neurite density measured with confocal microscopy in a cleared mouse brain.

Materials and Methods

Sample preparation

All animal protocols were approved by the institutional animal care and use committee of Juntendo University (Approval number: 280190). We used one young adult male thy-1 yellow fluorescent protein (YFP) 16 mouse (available from The Jackson Laboratory, strain B6.Cg-Tg[Thy1-YFP]16Jrs/J). The mouse was deeply anesthetized by isoflurane inhalation and intraperitoneal injections of pentobarbital, and then perfused with 25 ml of a heparinized (10 U/ml) ice-cold phosphate-buffered saline (PBS) solution followed by 25 ml of an ice-cold 4% paraformaldehyde (PFA) solution. The brain was carefully dissected out and fixed in 4% PFA solution for one day and then embedded in 1% agarose.

MRI data acquisition

Whole-brain MRI was acquired with a 7T animal MRI system (Agilent Technologies Inc., Palo Alto CA, USA) equipped with transmit/receive (TX/RX) 1H imaging channels and a 1 kW radio-frequency (RF) amplifier. The gradient coil (SGRAD 305/210/HD/S; Magnex Scientific Ltd., Abingdon, UK) had an inner diameter of 210 mm with a maximum gradient strength of 200 mT/m, and a linear region (±6%) of 12.0 cm. A four-turn solenoid coil was used to acquire the images. The inner diameter and length of the coil were 17 and 20 mm, respectively.

Diffusional kurtosis imaging and DTI were obtained using a 3D diffusion-weighted fast spin echo sequence with the following parameters: TR = 300 ms; echo train length = 4; TE = 31.86 ms; two averages; FOV, 19.2 mm × 19.2 mm × 19.2 mm; matrix size, 128 × 128 × 128. This yielded an image with 150 µm isotropic voxels. Initial b = 0 s/mm^2 and b = 1000, 2000 s/mm^2 images (δ = 8 ms, Δ = 13.0 ms) with 30 different diffusion directions corresponding to the Jones 30 scheme were acquired.[21] Total imaging time was 42 h 20 min.

Diffusion metric analysis

The diffusion MRI data were corrected for eddy current distortions and inter-volume subject motion using EDDYCORRECT implemented in the FMRIB Software Library 5.0.9 (FSL, Oxford Centre for Functional MRI of the Brain, Oxford, UK, www.fmrib.ox.ac.uk/fsl).[22] The data were processed using the Diffusional Kurtosis Estimator,[23] and the maps of mean kurtosis (MK), axial kurtosis (AK), and radial kurtosis (RK) were generated. The diffusion tensor was estimated using ordinary least squares applied to the b = 0 and b = 1000 s/mm^2 images, then mean diffusivity (MD), axial diffusivity (AD), radial diffusivity (RD), and fractional anisotropy (FA) were calculated.

Brain clearing and confocal microscopy

After scanning MRI, the brain was sectioned at a thickness of 2 mm and then cleared using the clear, unobstructed brain imaging cocktails and computational analysis (CUBIC) method,[24] incubating the sections in Sca*l*eCUBIC-1 mixture for 3 days, washing in PBS overnight, and then incubating in Sca*l*eCUBIC-2 mixture for 3 days.

Confocal microscopy was performed with a Carl Zeiss LSM 780 two-photon microscope (Carl Zeiss Meditec, Oberkochen, Germany) and a two-photon laser, wavelength, 920 nm (Chameleon; Coherent, Santa Clara CA, USA) equipped with a ×10 objective (numerical aperture, 0.45; working distance, 2 mm) (Plan Apochromat; Carl Zeiss Meditec). Acquired images were in 16-bit tiff format with the following voxel dimensions (µm): x, 1.66; y, 1.66; z, 4.

Region of interest analysis

Forty-eight ROIs were set on the caudate putamen (Fig. 1), seven ROIs were on the anterior commissure (Fig. 2a),and seven ROIs on the ventral hippocampal commissure (Fig. 2b) in a confocal microscopic image. The ROI size was 300 µm × 300 µm × 300 µm in the caudate putamen and 150 µm × 150 µm × 150 µm in the anterior commissure and the ventral hippocampal

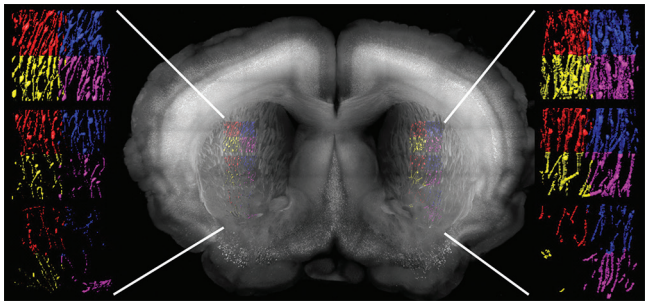

Fig. 1 Confocal microscopic image of the caudate putamen. Forty-eight ROIs were set on the caudate putamen in a confocal microscopic image. Twenty-four ROIs were placed on one coronal section and another 24 ROIs were placed on the adjacent section and the neurite density was calculated. The different colors were used only to highlight the borders of each ROI.

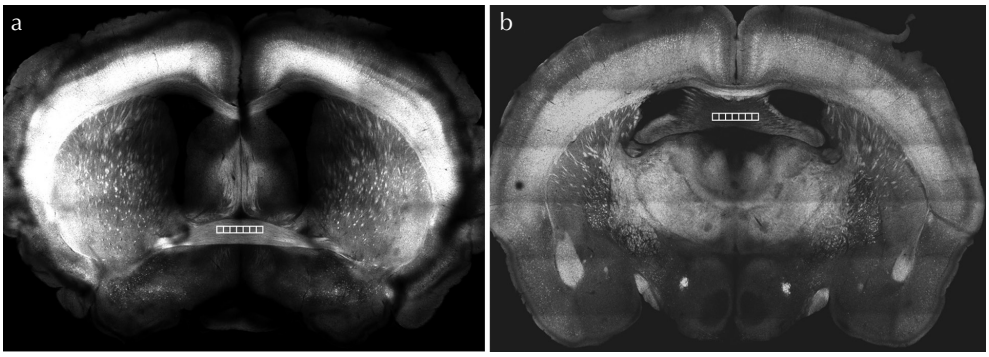

Fig. 2 Confocal microscopic images of the regions with well-aligned nerve fibers. Seven ROIs were set on the anterior commissure (**a**), and seven ROIs on the ventral hippocampal commissure (**b**). White frames show ROIs.

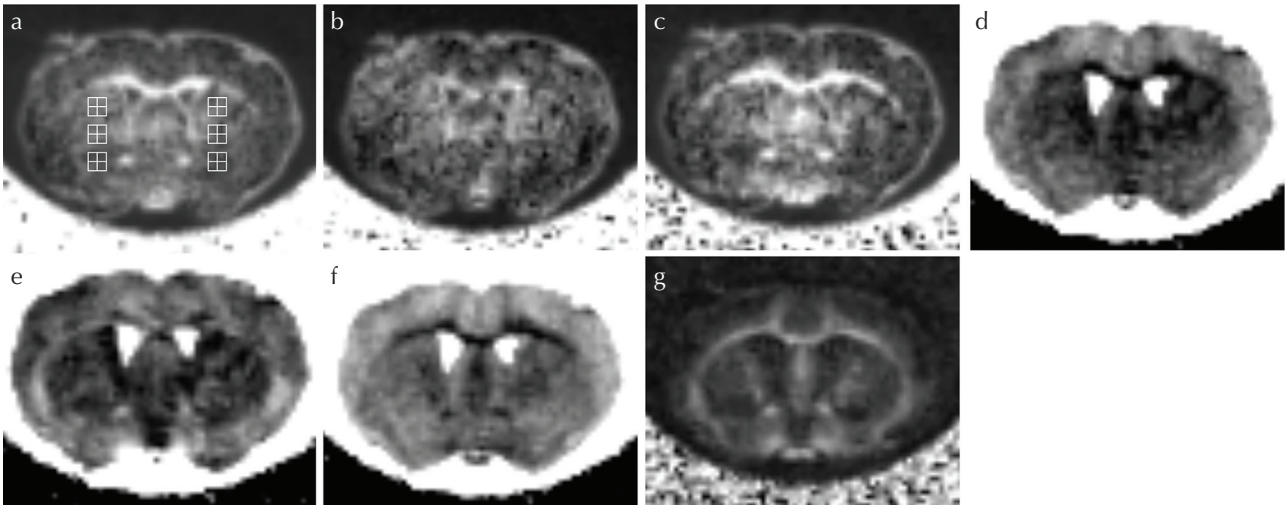

Fig. 3 Diffusion MRI maps of the caudate putamen. The maps of mean kurtosis (MK, **a**), axial kurtosis (AK, **b**), radial kurtosis (RK, **c**), mean diffusivity (MD, **d**), axial diffusivity (AD, **e**), radial diffusivity (RD, **f**), and fractional anisotropy (FA, **g**) were calculated. We manually identified the ROIs on the diffusion MRI map that corresponded to each ROI on the confocal microscopic image. White frames on the MK map show ROIs and we put ROIs at the same place on the other maps as on the MK map.

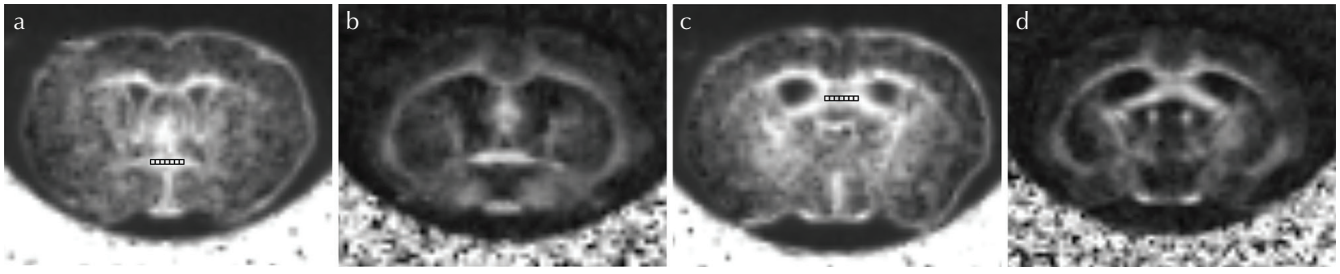

Fig. 4 Diffusion MRI maps of the regions with well-aligned nerve fibers. The coronal section of diffusion MRI maps at the level of the anterior commissure (mean kurtosis [MK], **a**; fractional anisotropy [FA], **b**) and the ventral hippocampal commissure (MK, **c**; FA, **d**) were calculated. We manually identified the ROIs on the diffusion MRI map that corresponded to each ROI on the confocal microscopic image. Black frames on the MK map show ROIs and we put ROIs at the same place on FA map.

commissure. In each ROI, histological neurite density was calculated using commercial software (Imaris Interactive Microscopy Image Analysis software, Bitplane, Zurich, Switzerland) with a threshold-based surface reconstruction. Dark soma regions were discarded from the data and the threshold was slightly adjusted according to the microscopic image intensity (manual threshold over 2000 in grey value, number of voxels above 1000). We manually matched the ROIs on the diffusion MRI map that corresponded to each ROI on the confocal microscopic image (Figs. 3 and 4).

Statistical analysis

The correlations between the diffusion metrics and neurite density measured in each ROI were analyzed by Pearson correlation

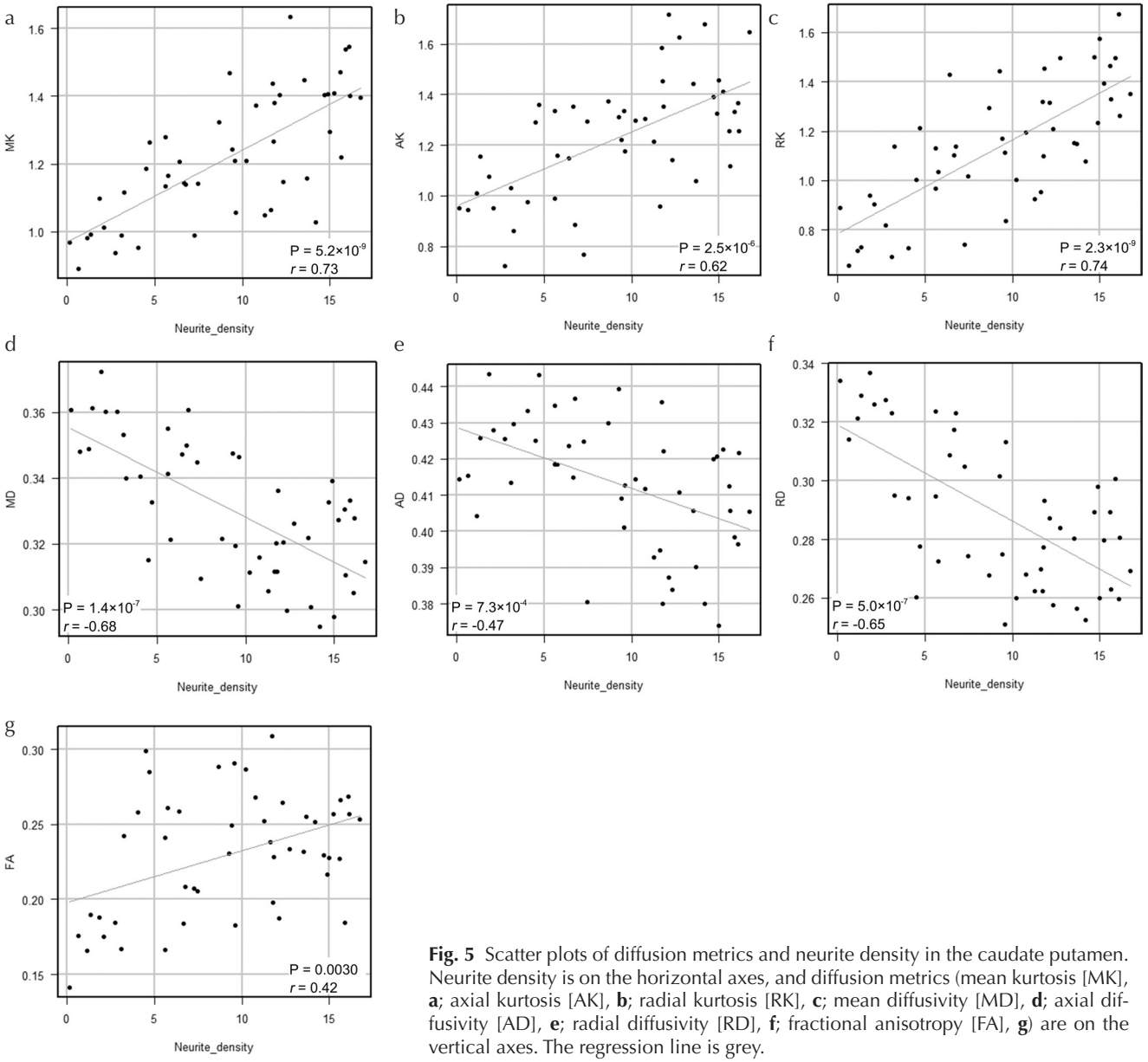

Fig. 5 Scatter plots of diffusion metrics and neurite density in the caudate putamen. Neurite density is on the horizontal axes, and diffusion metrics (mean kurtosis [MK], **a**; axial kurtosis [AK], **b**; radial kurtosis [RK], **c**; mean diffusivity [MD], **d**; axial diffusivity [AD], **e**; radial diffusivity [RD], **f**; fractional anisotropy [FA], **g**) are on the vertical axes. The regression line is grey.

coefficient analysis. A value of *r* ranging from 0.00–0.20 was regarded as "very weak," > 0.20–0.40 as "weak," > 0.40–0.60 as "moderate," > 0.60–0.80 as "strong," and > 0.80–1.0 as "very strong." All statistical analyses were performed using EZR (version 1.31; Saitama Medical Center, Jichi Medical University, Saitama, Japan), a graphical user interface for R (version 3.2.2, R Foundation for Statistical Computing, Vienna, Austria).[25]

Results

There were strong positive correlations between neurite density and DKI parameters especially MK ($r = 0.73$) and RK ($r = 0.74$) in the caudate putamen. MD ($r = -0.68$) and RD ($r = -0.65$) showed strongly negative correlations between neurite density. There was only a moderate positive correlation between neurite density and FA ($r = 0.42$) (Fig. 5). In the anterior commissure and the ventral hippocampal commissure, MK were very high value and showed no significant correlation with neurite density (Fig. 6a). Meanwhile, neurite density and FA are very strongly correlated in these areas ($r = 0.90$) (Fig. 6b).

Discussion

The present study revealed a strong positive correlation between DKI parameters and neurite density in the caudate putamen. The DKI parameters are believed to reflect the complexity of tissue microstructure. As the caudate putamen has many crossing fibers in it, high neurite density of the

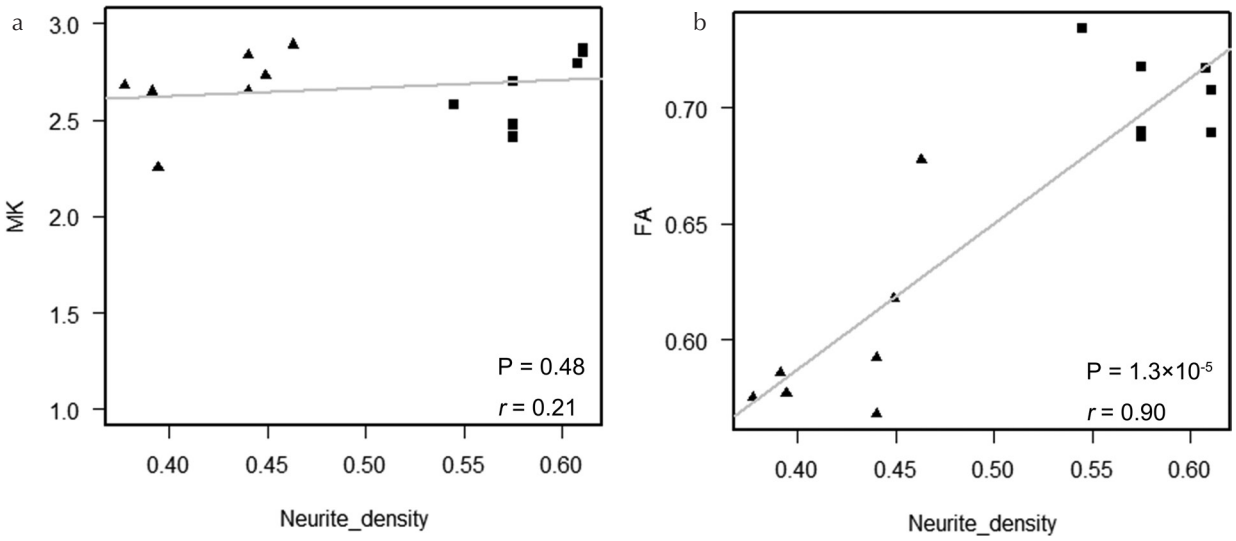

Fig. 6 Scatter plots of diffusion metrics and neurite density in the regions with well-aligned nerve fibers. Neurite density is on the horizontal axes, and diffusion metrics (mean kurtosis [MK], **a**; fractional anisotropy [FA], **b**) are on the vertical axes. Square plots showed results of the anterior commissure, and triangle plots showed results of the ventral hippocampal commissure. The regression line is grey.

caudate putamen means that the structure is complex. Our results confirmed that DKI correlated with neurite density of complex structures. In particular, RK correlated more strongly with neurite density than AK. MD and RD also showed strong correlation to neurite density. Radial diffusivity and kurtosis are generally assumed to reflect axon density, and that is consistent with our result.

Kamagata et al. reported that FA was very strongly correlated with neurite density in an area where nerve fiber orientations are unidirectionally aligned, such as the medial lemniscus.[26] In this study, FA showed very strong correlation with neurite density in the anterior commissure and the ventral hippocampal commissure where fiber orientations are well aligned, but did not strongly correlate with neurite density in the caudate putamen. These structures contain crossing fibers, whose evaluation by DTI is limited. FA values were lower in the areas with crossing fibers than the neurite density estimated on confocal microscopy. Therefore, DKI appears to be more sensitive than DTI in the evaluation of complex structures. On the other hand, MK were too high to evaluate neurite density in the regions with dense and well-aligned fibers such as anterior commissure and ventral hippocampal commissure.

There are some potential limitations in this study. The neurite density and complexity are not only the causes that have an influence on the DKI parameters. A change in myelination is a factor to influence the DKI results,[18] but it is difficult to discriminate between axon and myelin with confocal microscopy in a cleared mouse brain. It is also difficult to differentiate the cell species or structures. Projection neurons of the caudate putamen consists mostly of medium spiny neuron that has dense dendritic spines, and some interneurons also present.[27] A thy1-YFP-16 mouse expresses yellow fluorescent protein in almost all motor and sensory neurons, including somata, nuclei, axons, dendrites, and dendritic spines.[28] As a region with well-aligned fibers, we also tried to analyze the corpus callosum in the same way as used in the other regions. However, the results of the corpus callosum were not consistent. That was probably because the object was too small to measure, and the fluorescence in a confocal microscopy seems artificially low when close to the ventricle. We analyzed only one mouse in this study and it could be a limitation. However, it is practically impossible to scan more than one mouse in a completely same condition, so we considered that our study with one sample was reasonable. Regarding the method of our analysis, ROIs were set manually on the confocal microscopic images and the diffusion MR images, an accurate automatic image registration method for these two modalities is needed. The sample brain had been expanded with CUBIC method, so an existing software does not have a way to register the sample with an MR image scanned before CUBIC. We might be able to register them with some landmarks set, but a manual procedure is needed also in this way. Also, an appropriate quantifiable parameter of complexity or intersection property in confocal microscopy is needed to allow comparison with various parameters of diffusion MR images. The relatively low b-value might be a limitation of this study. High b-value is better to evaluate samples *ex vivo*, but our scans of high b-value were inconsistent to calculate diffusion metrics may be due to a severe artifact. To explore the microstructure of the brain, q-space imaging is another method and should be considered in the future study.

Conclusion

MK and RK were strongly correlated with neurite density in the caudate putamen. DKI accurately reflected neurite

density in these areas, which contain crossing fibers, potentially allowing evaluation of complex microstructures.

Acknowledgments

This work was supported by the program for Brain Mapping by Integrated Neurotechnologies for Disease Studies (Brain/MINDS) from the Japan Agency for Medical Research and Development (AMED), supported by JSPS KAKENHI Grant Number JP16H06280, supported by grants from the MEXT-Supported Program for the Strategic Research Foundation at Private Universities (2011–2015), and supported by ImPACT Program of Council for Science, Technology and Innovation (Cabinet Office, Government of Japan).

Conflicts of Interest

SY, YO and HO are employees of Hitachi Ltd., KT is an employee of Araya Brain Imaging. The other authors have no conflicts of interest.

References

1. Jensen JH, Helpern JA. MRI quantification of non-Gaussian water diffusion by kurtosis analysis. NMR Biomed 2010; 23:698–710.
2. Hori M, Fukunaga I, Masutani Y, et al. Visualizing non-Gaussian diffusion: clinical application of q-space imaging and diffusional kurtosis imaging of the brain and spine. Magn Reson Med Sci 2012; 11:221–233.
3. Raab P, Hattingen E, Franz K, Zanella FE, Lanfermann H. Cerebral gliomas: diffusional kurtosis imaging analysis of microstructural differences. Radiology 2010; 254:876–881.
4. Van Cauter S, Veraart J, Sijbers J, et al. Gliomas: diffusion kurtosis MR imaging in grading. Radiology 2012; 263: 492–501.
5. Jensen JH, Falangola MF, Hu C, et al. Preliminary observations of increased diffusional kurtosis in human brain following recent cerebral infarction. NMR Biomed 2011; 24:452–457.
6. Hori M, Aoki S, Fukunaga I, Suzuki Y, Masutani Y. A new diffusion metric, diffusion kurtosis imaging, used in the serial examination of a patient with stroke. Acta Radiol Short Rep 2012; 1:1–3. doi.org/10.1258/arsr.2011.110024
7. Hui ES, Fieremans E, Jensen JH, et al. Stroke assessment with diffusional kurtosis imaging. Stroke 2012; 43: 2968–2973.
8. Shimoji K, Uka T, Tamura Y, et al. Diffusional kurtosis imaging analysis in patients with hypertension. Jpn J Radiol 2014; 32:98–104.
9. Weber RA, Hui ES, Jensen JH, et al. Diffusional kurtosis and diffusion tensor imaging reveal different time-sensitive stroke-induced microstructural changes. Stroke 2015; 46:545–550.
10. Kazumata K, Tha KK, Narita H, et al. Characteristics of diffusional kurtosis in chronic ischemia of adult moyamoya disease: comparing diffusional kurtosis and diffusion tensor imaging. AJNR Am J Neuroradiol 2016; 37:1432–1439.
11. Yoshida M, Hori M, Yokoyama K, et al. Diffusional kurtosis imaging of normal-appearing white matter in multiple sclerosis: preliminary clinical experience. Jpn J Radiol 2013; 31:50–55.
12. Doring TM, Lopes FC, Kubo TT, et al. Neuromyelitis optica: a diffusional kurtosis imaging study. AJNR Am J Neuroradiol 2014; 35:2287–2292.
13. Serulle Y, Pawar RV, Eubig J, et al. Diffusional kurtosis imaging in hydrocephalus. Magn Reson Imaging 2015; 33:531–536.
14. Nakanishi A, Fukunaga I, Hori M, et al. Microstructural changes of the corticospinal tract in idiopathic normal pressure hydrocephalus: a comparison of diffusion tensor and diffusional kurtosis imaging. Neuroradiology 2013; 55:971–976.
15. Kamiya K, Kamagata K, Miyajima M, et al. Diffusional kurtosis imaging in idiopathic normal pressure hydrocephalus: correlation with severity of cognitive impairment. Magn Reson Med Sci 2016; 15:316–323.
16. Kamagata K, Tomiyama H, Motoi Y, et al. Diffusional kurtosis imaging of cingulate fibers in Parkinson disease: comparison with conventional diffusion tensor imaging. Magn Reson Imaging 2013; 31:1501–1506.
17. Kamagata K, Tomiyama H, Hatano T, et al. A preliminary diffusional kurtosis imaging study of Parkinson disease: comparison with conventional diffusion tensor imaging. Neuroradiology 2014; 56:251–258.
18. Kelm ND, West KL, Carson RP, Gochberg DF, Ess KC, Does MD. Evaluation of diffusion kurtosis imaging in *ex vivo* hypomyelinated mouse brains. Neuroimage 2016; 124:612–626.
19. Falangola MF, Guilfoyle DN, Tabesh A, et al. Histological correlation of diffusional kurtosis and white matter modeling metrics in cuprizone-induced corpus callosum demyelination. NMR Biomed 2014; 27:948–957.
20. Kerever A, Kamagata K, Yokosawa S, et al. See-through brains and diffusion tensor mri clarified fiber connections: a preliminary microstructural study in a mouse with callosal agenesis. Magn Reson Med Sci 2015; 14:159–162.
21. Jones DK, Horsfield MA, Simmons A. Optimal strategies for measuring diffusion in anisotropic systems by magnetic resonance imaging. Magn Reson Med 1999; 42:515–525.
22. Jenkinson M, Bannister P, Brady M, Smith S. Improved optimization for the robust and accurate linear registration and motion correction of brain images. Neuroimage 2002; 17:825–841.
23. Tabesh A, Jensen JH, Ardekani BA, Helpern JA. Estimation of tensors and tensor-derived measures in diffusional kurtosis imaging. Magn Reson Med 2011; 65:823–836.
24. Susaki EA, Tainaka K, Perrin D, et al. Whole-brain imaging with single-cell resolution using chemical cocktails and computational analysis. Cell 2014; 157: 726–739.

25. Kanda Y. Investigation of the freely available easy-to-use software 'EZR' for medical statistics. Bone Marrow Transplant 2013; 48:452–458.
26. Kamagata K, Kerever A, Yokosawa S, et al. Quantitative histological validation of diffusion tensor MRI with two-photon microscopy of cleared mouse brain. Magn Reson Med Sci 2016; 15:416–421.
27. Nisenbaum ES, Wilson CJ. Potassium currents responsible for inward and outward rectification in rat neostriatal spiny projection neurons. J Neurosci 1995; 15:4449–4463.
28. Feng G, Mellor RH, Bernstein M, et al. Imaging neuronal subsets in transgenic mice expressing multiple spectral variants of GFP. Neuron 2000; 28:41–51.